Article

Microbe-assisted fabrication of circularly polarized luminescent bacterial cellulosic hybrids
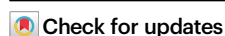
Yongjie Sun[1], Dan Zhang[1], Zhiqiang Dong[1], Jinxiao Lyu[1], Chunfei Wang[1], Jun Gong[1], Koon Ho Wong [1,2] ✉, Changfeng Wu [3] ✉ & Xuanjun Zhang [1,2] ✉

The fabrications of circularly polarized luminescent (CPL) material are mainly based on the chemical and physical strategies. Controlled biosynthesis of CPL-active materials is beset with difficulties due to the lack of bioactive luminescent precursors and bio-reactors. Enlighted by microbe-assisted asymmetric biosynthesis, herein, we show the in situ bacterial fermentation of *Komagataeibacter sucrofermentants* to fabricate a series of bacterial cellulosic biofilms with CPL of green, orange, red, and near-infrared colors. This process can trigger CPL emission for CPL-silent glycosylated luminophores and amplify the g_{lum} of weak CPL-active luminophores up to a 10^{-2} scale. To confirm glycosidic bonds formation during the bacterial copolymerization process, we develop an assay utilizing the cellulase-catalyzed biodegradation of BC hybrids. More importantly, we achieve the information encryption and Fe^{3+} dual-channel detection based on hybrid bacterial cellulosic biofilms. Therefore, this study not only provides another vision for CPL materials preparation but also broadens the application of bacterial cellulosic hybrids.

Ubiquitous chirality has gained significant attention for the development of circularly polarized chiroptical materials that exhibit extensive applications in optical storage[1,2], photoelectric devices[3–6], chiral sensors[7–11], chiroptical materials[12–16], and bioimaging[17]. In general, the preparation of circularly polarized luminescence (CPL) materials relies heavily on chemical and physical methods[18]. Chemical strategies involve the development of chiral fluorescent molecules and the incorporation of chiral moieties through covalent or coordinate bonds[19–24]. For instance, helical fluorescent molecules[20,25] and dyes based on chiral 1,1'-bi-2-naphthol[26] are known to be CPL-active, exhibiting g_{lum} ranging from 10^{-4} to 10^{-2}. Generally, the g_{lum} can be improved by increasing the molecular sizes or degree of distortion[27], but this greatly increases the synthesis workload and difficulty. Moreover, the CPL performance of the resulting chiral luminophores is often unpredictable[28]. Therefore, many researchers are exploring physical strategies to improve the CPL performance, which can offer a powerful solution to simplify the preparation process and precisely control the arrangement of building blocks, thereby enhancing certain properties. Assemblies[28–32], metal-organic frameworks (MOFs)[33,34], liquid crystals[35–38], and cellulose[39–41] are examples of physical systems that can form well-aligned and compact chiral structures. These structures can serve as a chiral platform for the formation of CPL-active materials through hydrogen bonding, π-π interactions, or adsorption. Such systems can induce excimer emission in the excited state[42,43], improve intramolecular exciton coupling interactions[44,45], or increase transition dipole moment vectors[46], ultimately enhancing the CPL performance. Unfortunately, the functional moieties in these systems are prone to collapsing or shedding upon external factors due to weak noncovalent bonding and physical interactions. Therefore, there is a strong demand for an efficient approach to fabricate stable CPL-active materials.

[1]Faculty of Health Sciences, University of Macau, Taipa, Macau SAR, China. [2]MOE Frontiers Science Center for Precision Oncology, University of Macau, Taipa, Macau SAR, China. [3]Department of Biomedical Engineering, Southern University of Science and Technology, Shenzhen, Guangdong, China. ✉e-mail: koonhowong@um.edu.mo; wucf@sustech.edu.cn; xuanjunzhang@um.edu.mo

Compared to chemical and physical strategies, biosynthesis[47–50] exhibits green, efficient, and mass-productive properties. Meanwhile, biosynthesis shows potential for chiral platform construction due to the abundant chiral components in living matter and nature, such as L-amino acids, D-sugars, peptides, and nuclei acids[51], while this strategy is rarely used in CPL material construction, as specialized bioreactors are needed. Bacterial synthesis, as a type of biosynthesis, offers tremendous potential for the preparation of biobased hybrid materials, which have now been applied to fuel cells, biological repair systems, and the field of synthetic biology[52,53]. Bacterial fermentation based on Acetobacter xylinus is extensively employed for the large-scale production of flexible bacterial cellulose (BC). Once glucose is taken up by the bacteria, it polymerizes through β-1,4-glycosidic bonds catalyzed by cellulose synthase. The resulting glucan chains then assemble and crystallize, forming bacterial cellulose with the help of intra- and intermolecular hydrogen bonds (Fig. 1a). Compared to many other polymeric or self-assembled materials, BC exhibits not only high porosity and water content and strong mechanical strength in wet conditions but also high degree of polymerization, a large specific surface area, low density, and excellent tunability[54]. These properties have laid the foundation for its use in paper production, the food industry, and wound dressing[54]. Recently, researchers have successfully developed bacterial fermentation of glycosylated molecules and D-glucose to form dye-hybrid BCs in situ[55–57], which can be used to visualize the bacterial copolymerization process and as engineered living material for skin wound repair, showing great significance to flexible applications of hybrid BCs. However, the bacterial copolymerization of various types of glycosylated molecular structures and linkages between

glucose and dyes have not been evaluated under the same culture conditions, and a general and efficient characterization method needs to be developed. More importantly, bacterial fermentation process has the ability to create a nanostructure with a right-handed twist[40,58], indicating its potential in constructing CPL-active materials.

In this study, using in situ bacterial fermentation of *Komagataeibacter sucrofermentans*, we create a series of fluorescent BC biofilms from glycosylated luminophores with different linkages and colors (Fig. 1b, c), showing excellent versatility. Importantly, we demonstrate that this process can trigger circularly polarized luminescence (CPL) emission in CPL-silent glycosylated dyes from green to red and near-infrared fluorescence with g_{lum} of -3.8×10^{-3} (S1-BC), -5.6×10^{-3} (S2-BC), -1.7×10^{-3} (S3-BC) and -3.4×10^{-3} (S4-BC) (Fig. 1b). It furthermore enhances the g_{lum} of weak CPL-active luminophores from the 10^{-4} scale to the 10^{-2} scale with as high as 39-fold amplification (Fig. 1c). Furthermore, this system improves the stability between luminophores and the chiral matrix through glycosidic bonds. To verify that chromophores can be covalently embedded into BC membranes via in situ copolymerization, we explore the cellulase-catalyzed biodegradation of BC hybrids to track the dye-hybrid glucose and oligosaccharides, and successfully detect dye-hybrid cellobiose, cellotriose, cellotetrose and cellopentaose by high-resolution mass spectrometry (HRMS) after biodegradation. In addition, we construct the templates of information encryption through microbe-assisted biosynthesis of photo-switching glycosylated molecule. Surprisingly, S4-BC can achieve ratiometric Fe^{3+} ion detection using both fluorescent and CPL channels with the assistance of S4. Taken together, we not only provide a biosynthetic
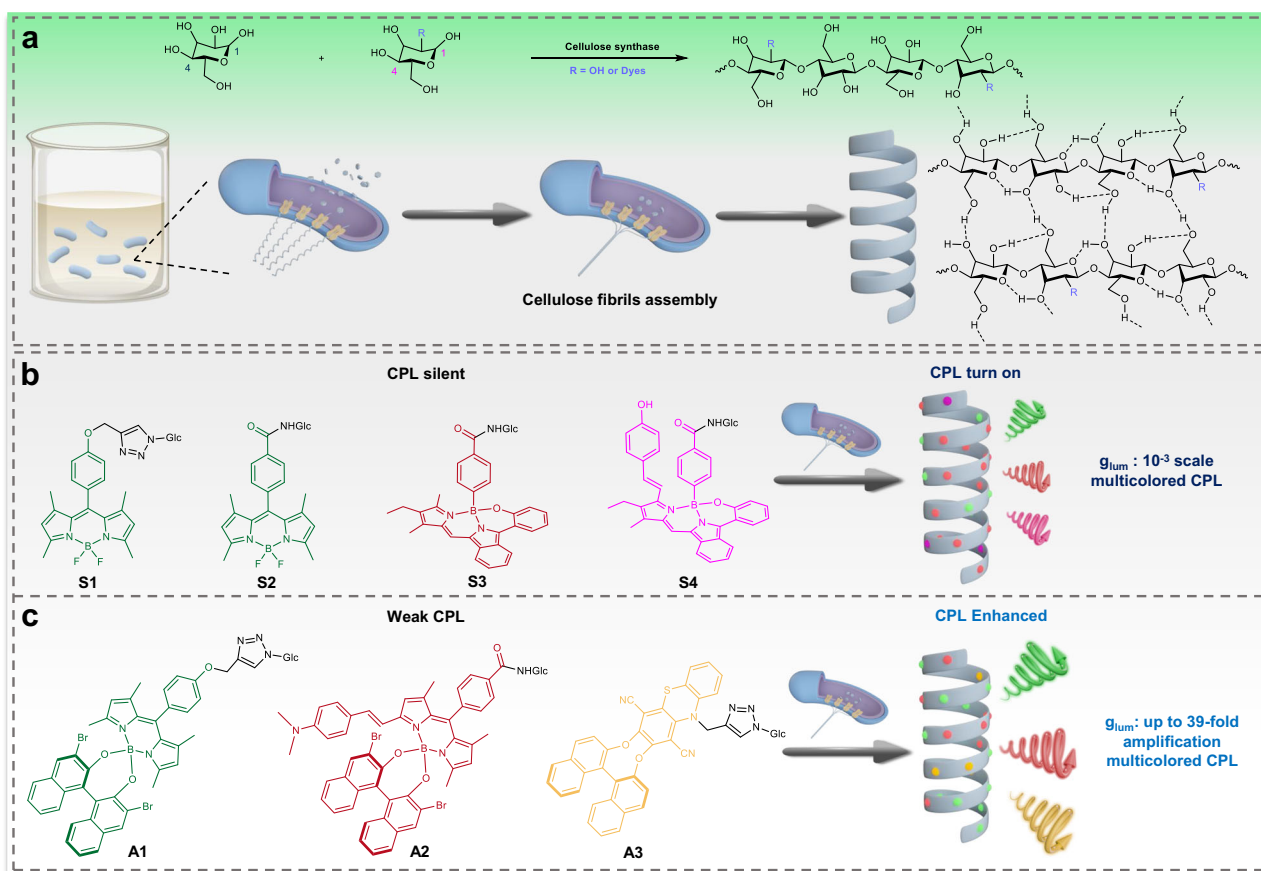

Fig. 1 | Schematic illustration of CPL-active bacterial cellulosic hybrids formation via bacterial fermentation. a Bacterial cellulose is created in situ through the β−1,4-glycosidic reaction catalyzed by cellulose synthase in bacteria. **b** The CPL-silent glycosylated molecules exhibit CPL emission when triggered by in situ bacterial fermentation. **c** The weak CPL-active glycosylated molecules experience an amplification of CPL performance after in situ bacterial fermentation. CPL, circularly polarized luminescence.
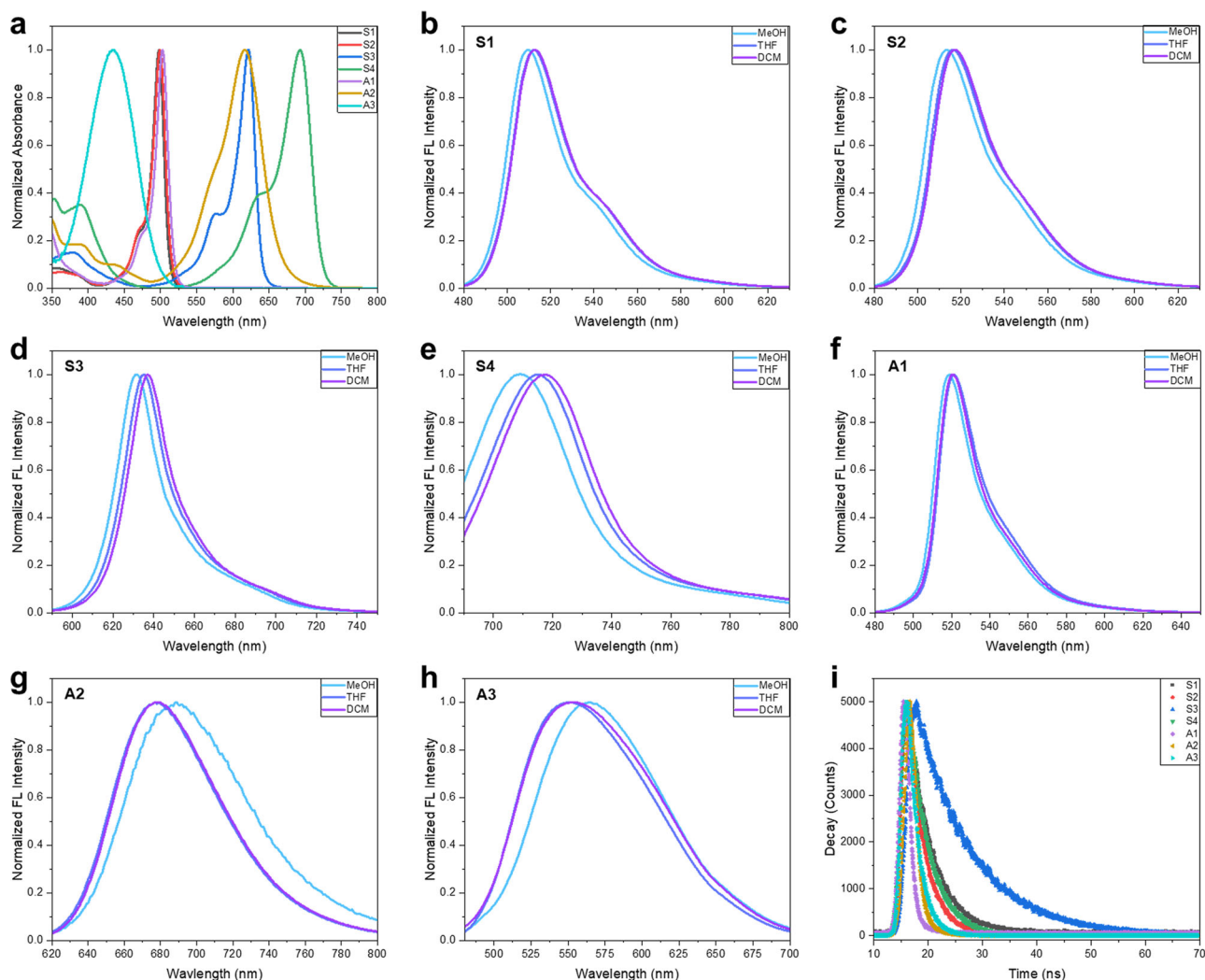
Fig. 2 | Photophysical properties of glycosylated molecules. a Normalized absorption spectrum S1-S4 and A1-A3 in diluted THF solution ($c = 10\,\mu M$). **b–h** Normalized FL emission spectra of S1-S4 and A1-A3 in different solvents (MeOH, THF, DCM) ($c = 10\,\mu M$). $\lambda_{ex} = 470$ nm for S1, S2 and A1, $\lambda_{ex} = 580$ nm for S3 and A2, $\lambda_{ex} = 680$ nm for S4, and $\lambda_{ex} = 430$ nm for A3. **i** Fluorescence lifetimes decay of S1-S4 and A1-A3 in EtOH diluted solvents ($c = 20\,\mu M$). THF tetrahydrofuran, MeOH methanol, DCM dichloromethane, FL fluorescence. Source data are provided as a Source Data file.

strategy for the preparation of stable CPL-active, photo-switching, and sensing materials but also develop a direct and efficient method for characterizing covalent bacterial copolymerization.

Results and discussion
Synthesis and characterization of biocompatible glycosylated dyes

To develop the bacterial copolymerization to form fluorescent bacterial cellulosic biofilms, biocompatible glycosylated dyes are needed. We designed and prepared the achiral luminophores M1 (green fluorescence), M2 (green fluorescence), M3 (red fluorescence), and M4 (near-infrared fluorescence), as well as the chiral luminophores M5 (green fluorescence), M6 (red fluorescence), M7 (orange fluorescence) and M8 (green fluorescence, photo-switching molecule) with alkynyl or carboxyl groups. Subsequently, click reaction and amidation were utilized to combine the luminophores with 2-azido-2-deoxy-*D*-glucose or 2-amino-2-deoxyglucose, forming the glycosylated luminophores with different linkages. The chemical structures and synthesis are detailed in the Supporting Information (Supplementary Figs. 1–8). The composition of each compound was fully characterized using ^{1}H NMR, ^{13}C NMR, and high-resolution mass spectrometry (HRMS).

Photophysical and chiroptical properties of glycosylated luminophores

The ultraviolet–visible (UV–Vis) spectra of glycosylated dyes were studied in diluted solutions. As shown in Fig. 2a, the S1, S2, and A1 dyes display similar absorbance spectra, as they are all based on boron-dipyrromethene (BODIPY) dyes with slight modifications. In detail, the maximum absorbance peaks are observed at 498, 499, and 503 nm, respectively. Additionally, A1 shows a slight redshift when compared to S1 due to the introduction of (*R*)-6,6′-dibromo-1,1′-bi−2-naphthol (*R*-Br-BINOL), which is consistent with the characteristics of intramolecular charge transfer (ICT)[59]. After condensation with 4-hydroxybenzaldehyde, the absorbance peak of S3 undergoes a bathochromic shift of 71 nm, from 622 nm to 693 nm (S4). In addition, A2 has a similar maximum absorbance peak as S3, located at 616 nm. In comparison to the previously mentioned glycosylated dyes, A3 exhibits the shortest wavelength at the maximum absorbance peak, which is situated at 435 nm. The emission properties of glycosylated dyes were evaluated in methanol (MeOH), tetrahydrofuran (THF), and dichloromethane (DCM) dilute solvents (Fig. 2b–h). With decreasing solvent polarity, S1-S4 and A1 show very little redshift in fluorescence emission spectra, while A2 and A3 display the hypochromatic shifts. In addition, the emission shifts of S3,

S4, A2, and A3 are more sensitive to solvent polarity than those of the others. Therefore, the introduction of a glucose moiety has a minimal impact on their absorptions and emissions. The absolute fluorescence quantum yield and lifetime of these glycosylated dyes were evaluated in ethanol (EtOH) diluted solutions (Fig. 2i and Supplementary Table 1). Among them, S1, S2, S3, and A3 exhibit good quantum yields, with S3 also showing a good lifetime.

The chiroptical properties of all glycosylated luminophores were evaluated in THF-diluted solutions. As shown in Fig. 3a–d, we studied the CPL performance of S1, S2, S3, and S4, which combine an achiral luminophore with a chiral glucose moiety, and found that they are all CPL-silent, probably because chirality transmission from the chiral glucose moiety to luminophores is difficult. On the other hand, A1 and A2 (which have the rigid chiral moiety of R-Br-BINOL) exhibit CPL-active emission in dilute THF solution with a g_{lum} of -7.7×10^{-4} at 520 nm and a g_{lum} of -1.3×10^{-3} at 679 nm, respectively, consistent with chiral BODIPY molecules in the solution state (Fig. 3e, f)[26,59]. Interesting, A3, based on S-BINOL, also performs CPL-active emission in dilute THF solution with a g_{lum} of -6.9×10^{-4} at 549 nm (Fig. 3g). In addition, the circular dichroism (CD) performance was similar to the CPL performance. S1, S2, S3, and S4 are CD-silent, while A1, A2, and A3 are CD-active (Supplementary Fig. 9).

Bacterial cellulosic biofilm formation through in situ bacterial fermentation

Firstly, the biocompatibility of these glycosylated molecules was evaluated (Supplementary Fig. 10). Compared to S3 and A2, S1, S2, S4, A1, and A3 exhibited higher biocompatibility. Among them, A2 showed worst biocompatibility. Subsequently, to fabricate fluorescent bacterial cellulosic biofilms through bacterial copolymerization, *Komagataeibacter sucrofermentants* were grown in culture medium containing glucose and glycosylated luminophores (S1, S2, S3, S4, A1, A2, and A3) (10 mg/100 mL medium). BC and hybrid BC biofilms were obtained after 6 days (12 days for A3) of incubation and were treated with NaOH aqueous solution (1%, w/v) to remove the residual medium and microorganisms. As shown in Fig. 4a, under natural light, BC, S1-BC, A1-BC, A2-BC, and A3-BC are colorless, while S2-BC, S3-BC, and S4-BC display slight orange, blue, and green appearances, respectively. Under UV light, all hybrid BC biofilms display fluorescence of the expected color: e.g., S1-BC, S2-BC, and A1-BC show green fluorescence, S3-BC, S4-BC and A2-BC display red fluorescence, and A3-BC show orange fluorescence (Fig. 4b), while it was observed that S3, S4, and A2 are nonfluorescent in the solid state (Supplementary Fig. 11). In addition, confocal Z-stack experiments demonstrated that the three-dimensional fluorescence data of hybrid BCs is derived from their complete membranes, except for any adsorption that takes place on their top and bottom surfaces (Fig. 4e). Taken together, the dyes are well distributed in the bacterial cellulosic nanofibers. All of the fluorescence information was confirmed by confocal laser scanning microscopy (CLSM) (Fig. 4c) and fluorescence emission spectroscopy (Supplementary Fig. 12). Besides, the absolute fluorescence quantum yields and lifetimes of all bacterial cellulosic biofilms were also evaluated (Supplementary Fig. 13 and Supplementary Table 2). Most of the glycosylated dyes experienced a decrease in quantum yields after bacterial fermentation, while their fluorescence lifetimes did not change significantly. Moreover, scanning electron microscopy (SEM) experiments demonstrated that there are no significant differences in the network structures of nanofibers between BC and BC hybrids (Fig. 4d), although there were slight differences in their thickness (Supplementary Fig. 14). Therefore, the embedding of glycosylated luminophores has little influence on the morphology of cellulose nanofibers. The highly ordered structure of bacterial cellulosic biofilms, characterized by intra- and intermolecular hydrogen bonding, results in poor solubility in most solvents. This makes direct evaluation of their molecular weights challenging. One of commonly used solvent system for producing bacterial cellulose solutions is a mixture of dimethylacetamide (DMAc) and lithium chloride (LiCl). To assess the molecular weights of the bacterial cellulosic hybrids, gel permeation chromatography (GPC) experiments were performed after dissolving the samples in the DMAc/LiCl mixture. The impressive molecular weights highlight the success of bacterial copolymerization (Supplementary Table 3).

Moreover, the hybrid BC biofilms show characteristic absorbance peaks that are relevant to corresponding glycosylated luminophores (Fig. 5a–g). For S1-BC, S2-BC, and A1-BC, the absorbance peaks appear at 503, 504, and 506 nm, respectively, consistent with that of the S1, S2, and A1 dyes in THF dilute solution with a slight redshift of 5, 7, and 4 nm, respectively. In addition, S3-BC and S4-BC show absorbance peaks at 630 nm and 707 nm, respectively, with redshifts of 12 and 16 nm, respectively, when compared to those of S3 and S4 in the solution state. However, due to the higher molecular weight and steric hindrance of the dyes A1, A2, and A3, their copolymerization efficiency is low, causing their absorbance peaks to be inconspicuous (Fig. 5e–g). The current-voltage experiments were conducted in a 0.1 nM KCl aqueous environment (pH = 7) to evaluate the electroconductivity of BC and bybrid BC biofilms (Fig. 5h). In the current-voltage curves, all hybrid BC biofilms show a smaller current than pure BC due to the increased hydrophobicity after the introduction of luminophores (Fig. 5i). These above results indicate that the glycosylated dyes were successfully embedded into bacterial cellulose with little influence (if any) on bacterial fermentation. Moreover, the two different linkers, triazole and amido linkages, appear to have minimal impact on bacterial copolymerization.

Amplification of chirality transfer and CPL performance

For small chiral organic molecules, the magnetic transition dipole moment (m) is often overshadowed by the electric transition dipole moment (μ). This, combined with their nonoptimized alignment (θ), results in very small g_{lum} (Eq. (1)). Additionally, the size of small organic molecules at their widest point is smaller than the hundreds of nanometers wavelengths of circularly polarized (CP) light at relevant energies, and therefore, they do not experience a significant degree of the twist of the light[27]. Notably, that assemblies with a helical twist structure can provide a chiral environment for achiral dyes to emit CP luminescence[28,60]. The helical pitch of chiral assemblies manifested over length scales can correspond to the wavelengths of their emission/absorption maxima, improving the distinction of the rotation of the light[27].

$$g_{lum} = \frac{I_L - I_R}{1/2\,(I_L + I_R)} = 4\cos\theta\,\frac{|m||u|}{|m|^2 + |u|^2} \approx 4\cos\theta\,\frac{|m|}{|u|} \tag{1}$$

Based on this perspective, we first evaluated the CPL performance of CPL-silent molecular (S1, S2, S3, and S4) BC biofilms. As shown in Fig. 6a–d, the four kinds of BC hybrids are CPL-active, exhibiting negative Δ intensity. In general, the Δ intensity originates from the intensity difference between left-handed CPL and right-handed CPL. Consequently, the BC hybrids emit right-handed CPL under our testing setup (Supplementary Fig. 15), which is due to efficient chirality transmission for the right-hand twisted structure of cellulose. S1-BC and S2-BC are CPL active in the green fluorescence window with g_{lum} of -3.8×10^{-3} (513 nm, Fig. 6a) and -5.6×10^{-3} (517 nm, Fig. 6b), respectively. In addition, S3-BC performs CPL in the red fluorescence window with a g_{lum} of -1.7×10^{-3} (640 nm, Fig. 6c) and S4-BC shows near-infrared CPL with a g_{lum} of -3.4×10^{-3} (715 nm, Fig. 6d), while BC is CPL-silent upon relevant excitation (Supplementary Fig. 16). These results indicate that the in situ bacterial copolymerization of glucose and glycosylated luminophores can help form a chiral environment in situ to trigger CPL emission of CPL-silent dyes.

To investigate the effect of chiral luminophores, we evaluated the CPL performance of A1-BC, A2-BC, and A3-BC obtained from the bacterial copolymerization of weak CPL molecules A1, A2 and A3,

respectively (Fig. 6e–g). To our surprise, A1-BC shows green CPL with a g_{lum} of -3×10^{-2} at 511 nm (Fig. 6e), performing 39-fold amplification of g_{lum} compared to that of A1 in THF solution (-7.7×10^{-4} at 520 nm). The
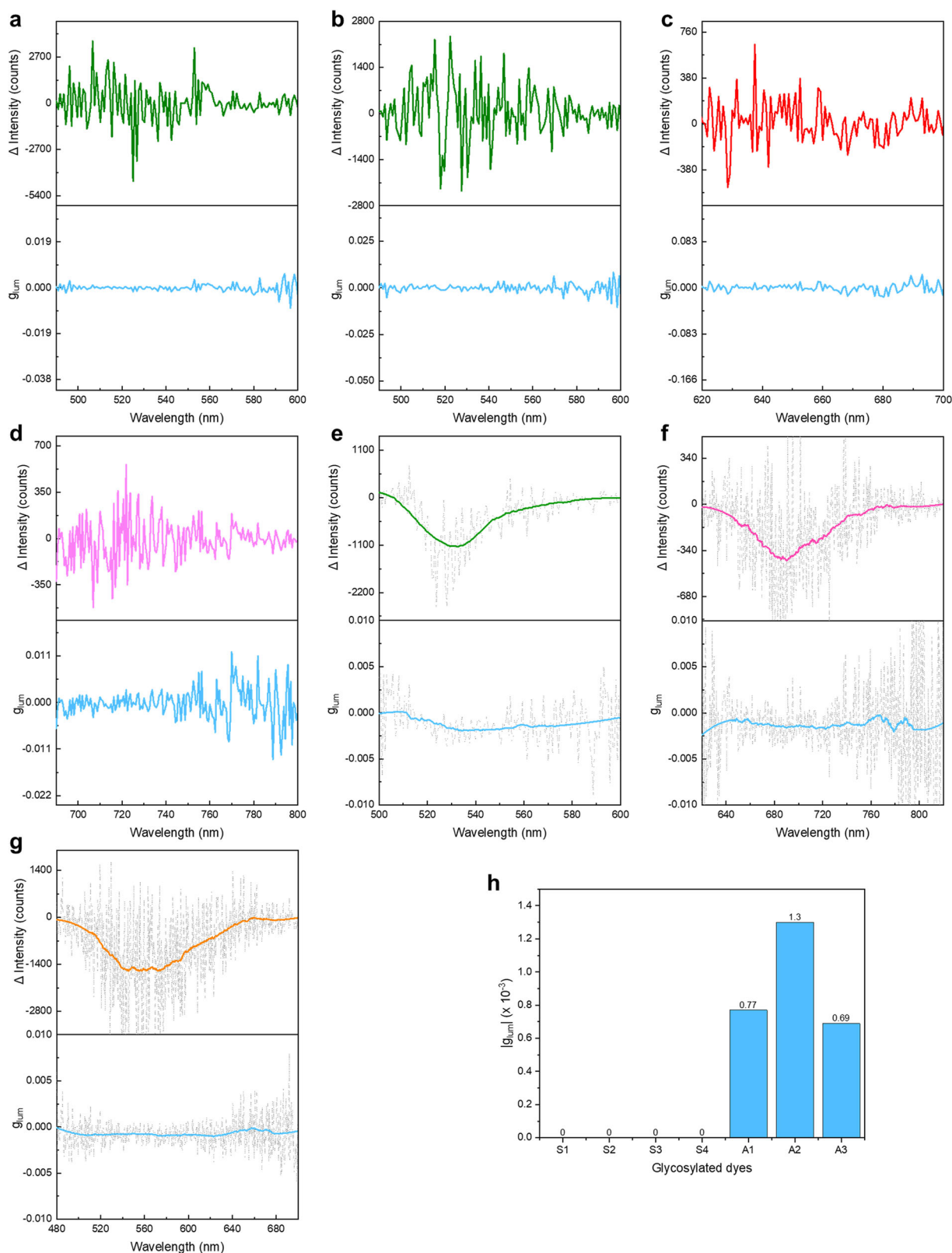

Fig. 3 | CPL spectra of glycosylated dyes in THF-diluted solution (c = 10 μM). For S1 (**a**), S2 (**b**), and A3 (**g**) λ_{ex} = 370 nm. For A1 (**e**), λ_{ex} = 450 nm. For S3 (**c**), λ_{ex} = 500 nm. For S4 (**d**), λ_{ex} = 650 nm, and for A2 (**f**), λ_{ex} = 580 nm. **h** Summary of g_{lum} of glycosylated dyes in THF-diluted solution. (**e–g** the gray dot curves are the original collected data, while the solid curves are the smoothed ones.) THF tetrahydrofuran. Source data are provided as a Source Data file.
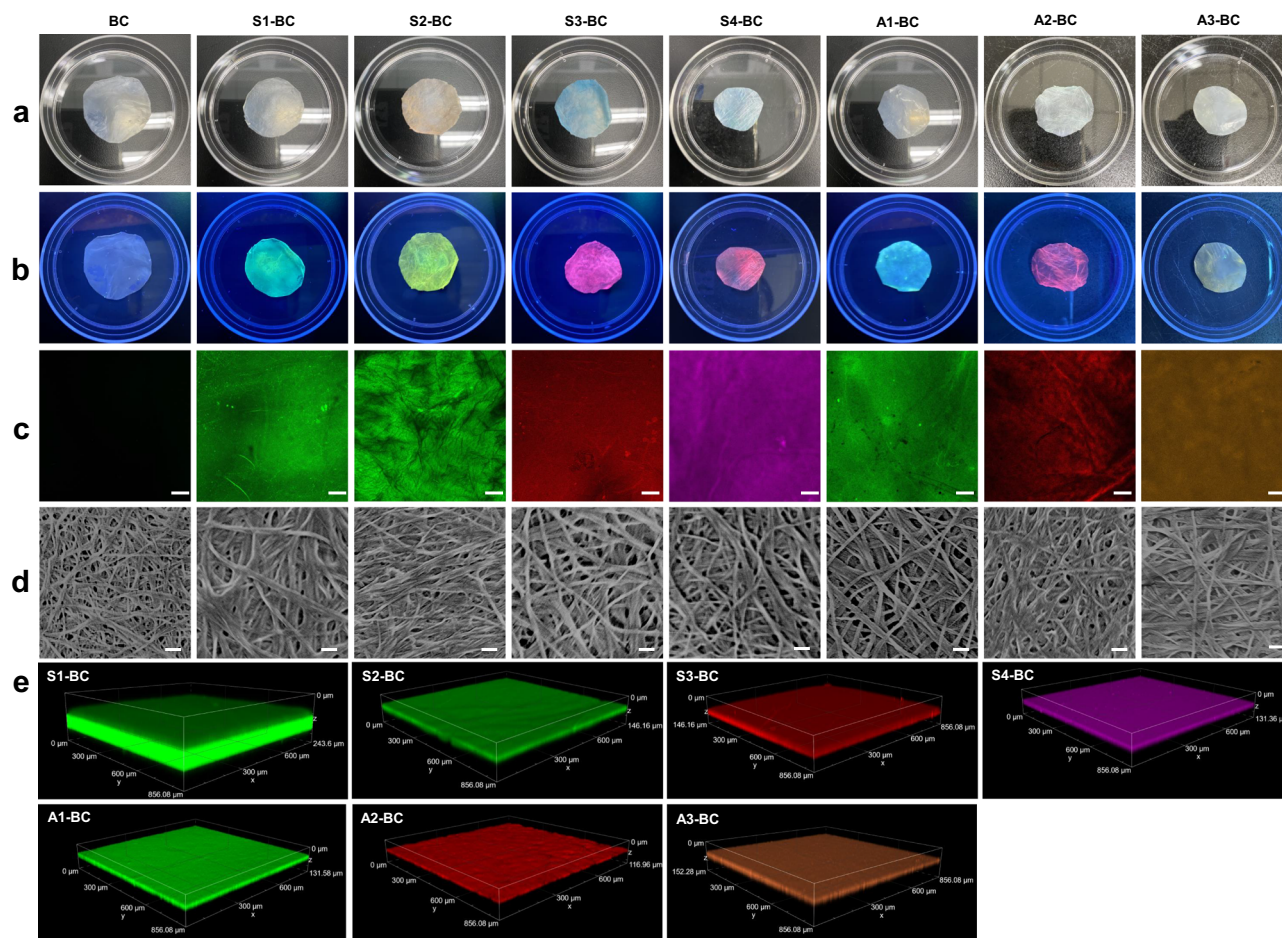
Fig. 4 | Characterization of bacterial cellulosic biofilms. Recorded images of BC and hybrid BC biofilms under natural light (**a**), 365 nm UV light (**b**) and CLSM (**c** scale bar: 100 μm), **d** Microstructure observation of BC and hybrid BC biofilms through SEM (scale bar: 200 nm). **e** CLSM three-dimensional fluorescence information of hybrid BCs. CLSM and SEM experiments were repeated three times independently with similar results. BC bacterial cellulose, UV ultraviolet, CLSM confocal laser scanning microscope, SEM scanning electron microscope. Source data are provided as a Source Data file.

CPL performance of A2 is also enhanced from -1.3×10^{-3} to -8.2×10^{-3} (Fig. 6f) along with ~6-fold amplification. In addition, A3-BC displays orange CPL with a g_{lum} of -1.52×10^{-2} (Fig. 6g), performing 22-fold amplification. The enhanced CPL performance benefits from the chirality transmission from BC and chiral BINOL moiety. Combined with the results of S1-BC, our results demonstrate that BC can amplify the chirality transmission from chiral *R*-Br-BINOL. Based on the above results, in situ bacterial fermentation can be used to enhance the g_{lum} of weakly CPL-active glycosylated dyes.

Covalent bond formation during bacterial copolymerization

In general, bacterial production of BCs and dye-hybrid BCs involves three steps with the assistance of specific operons and enzymes: (1) polymerization of glucose monomers to form poly-*D*-glucan chains, (2) extracellular transport and assembly of poly-*D*-glucan chains into cellulose fibrils, and (3) crystallization of cellulose fibrils into a highly ordered network structure[61] (Fig. 1a). Although bacterial fermentation has been used for the in situ introduction of dyes or photosensitive molecules into bacterial cellulose[55–57], there is no direct evidence for the characterization of glucosidic bond formation between glucose and glycosylated luminophores. Cellulase, combining endoglucanase, exoglucanase, and β-glucosidase, can biodegrade BCs to glucose and oligosaccharides under suitable conditions[62]. To investigate glucosidic bond formation, we conducted biodegradation experiments on bacterial cellulosic hybrids (S2-BC and S3-BC) and were able to detect dye-functionalized glucose or oligosaccharides by mass spectrometry

(Fig. 7a). As shown in Fig. 7b c and Supplementary Fig. 17, in addition to glucose, S2 and S2-hybrid cellobiose and cellotriose were the main components of the hydrolysate of S2-BC. Moreover, for the hydrolysate of S3-BC, S3-hybrid cellobiose, cellotriose, cellotetraose, and cellopentaose were detected. Combined with the fluorescence spectra of the hydrolysate (Fig. 7b left and 7c left), we demonstrate that the glycosylated dyes were successfully and stably inserted into the bacterial cellulose through covalent bonds.

Information encryption by photo-switching bacterial cellulosic biofilm

Dithienylethenes serve a broad range of applications in memory storage, switches, and actuators[63–65]. Leveraging the properties of dithienylethenes, scientists have successfully synthesized an extensive array of fluorescence-switching molecules[66–68]. In this study, we combined dansyl chloride and dithienylethene to prepare a fluorescent glycosylated photo-switching molecule, PS-Glc (Supplementary Figs. 8 and 18). When exposed to UV light (254 nm), dithienylethene moiety undergoes cyclization to form a non-fluorescent structure, which acts as the energy acceptor to quench the fluorescence of the dansyl moiety. However, upon irradiation with visible light (590 nm), the fluorescence is revived due to the ring-opening process, restricting the Förster resonance energy transfer (FRET) process (Fig. 8a and Supplementary Fig. 19). Moreover, PS-Glc showed minimal restriction on bacterial growth, indicating its potential as a candidate for use in bacterial fermentation (Supplementary Fig. 20). Following bacterial fermentation,
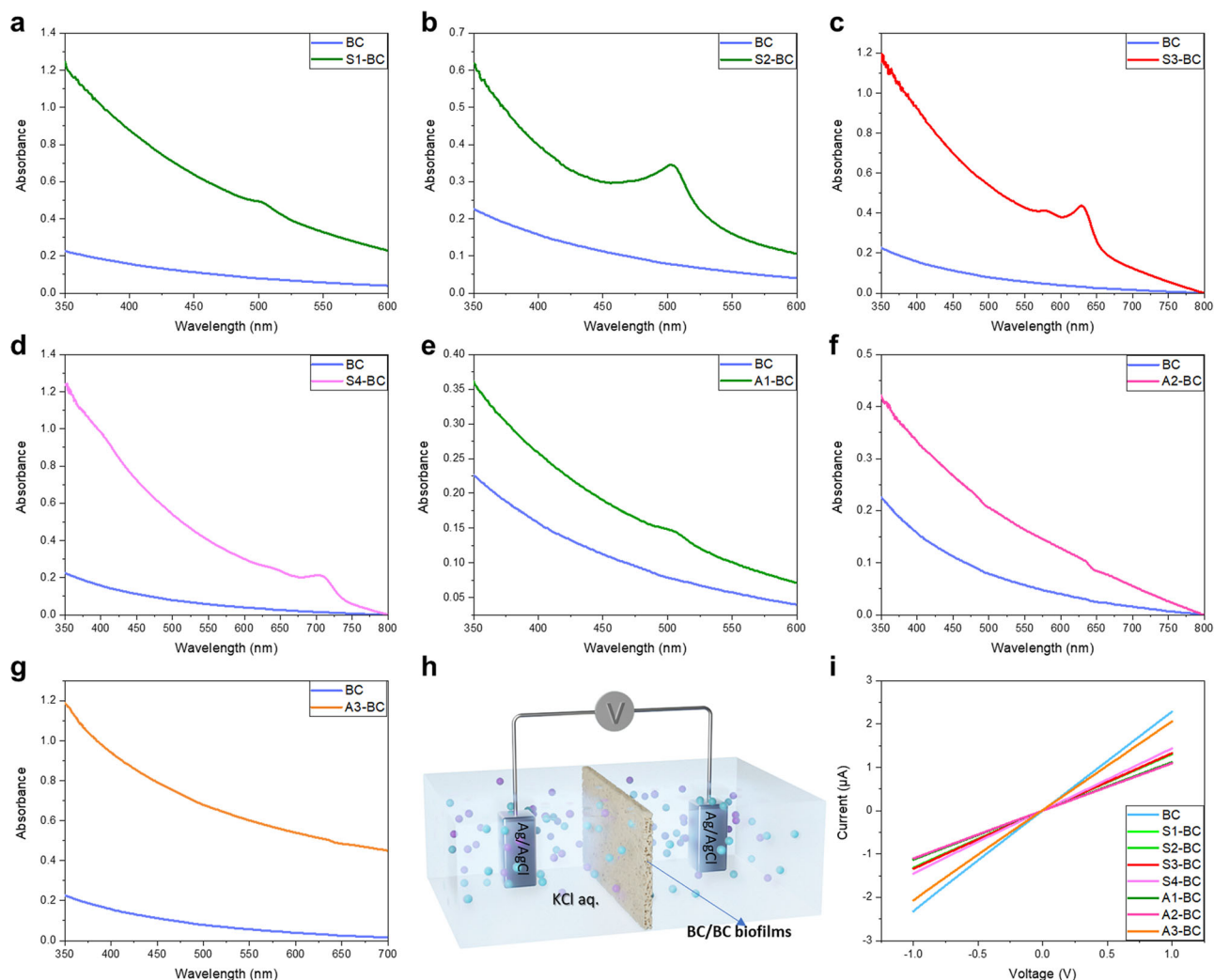
Fig. 5 | Properties of absorbance and current-voltage experiments for bacterial cellulosic biofilms. a–g Absorbance spectra of BC and hybrid BC biofilms. **h** Schematic representation of the transmembrane current experiment. **i** Current-voltage curves of BC and hybrid BC biofilms. BC bacterial cellulose. Source data are provided as a Source Data file.

we successfully fabricated the PS-Glc hybrid BC (PS-BC) biofilm (Fig. 8a and Supplementary Fig. 21). Impressively, the PS-BC biofilm retains the optical switching characteristics of PS-Glc (Supplementary Fig. 22). Utilizing the light-induced fluorescence changes of the PS-BC biofilm, we proposed information encryption models (Fig. 8b–d). As depicted in Fig. 8b, we realized the photoetching-erasure process for information encryption. Upon exposure to 254 nm light, "UM" can be inscribed on the biofilm, exhibiting non-fluorescence, which was then erased following 590 nm light irradiation. Subsequently, the fluorescent "FHS" can be inscribed upon it using 254 nm photoetching, displaying the photo-switching properties of PS-BC. Additionally, quick response (QR) codes for information storage can also be achieved through a similar photoetching method (Fig. 8c, Supplementary Fig. 23, and Supplementary Movie). Moreover, by combining S2-BC, PS-BC, and BC, we accomplished 8-bit ASCII (American Standard Code for Information Interchange) information encryption (Fig. 8d). Prior to 254 nm light irradiation, the incorrect information "917 = " was read out, as both PS-BC and S2-BC exhibit green fluorescence. However, after 254 nm light irradiation, the correct information "1069" was revealed as a result of the fluorescence quenching of PS-BC. Consequently, the information encryption utilizing photo-switching bacterial cellulosic hybrids has been successfully implemented.

Fluorescent and circularly polarized luminescent dual-sensing Fe³⁺ ions base on S4-BC

Recently, chiroptical probes have garnered significant attention in bio-species detection due to their high specificity[7–10,69,70]. To date, several highly selective probes have been developed for the detection and sensing of Fe^{3+} ions. However, the number of turn-on or ratiometric fluorescent probes for Fe^{3+} ion detection remains limited due to its strong paramagnetic quenching nature. Not to mention the CPL probes. Our group has discovered that the alkene C=C bond of near-infrared *N,N,O*-type benzopyrromethene boron complexes (BOBPYs) can undergo oxidative cleavage to form a red fluorescent compound[71], which realizes the ratiometric fluorescence change. Herein, we found that the glycosylated near-infrared BOBPY (S4) can response Fe^{3+} ions through the alkene oxidative cleavage, demonstrating good selectivity (Supplementary Fig. 24). However, the formed compound was CPL-silent in solution due to insufficient chirality transfer (Supplementary Fig. 25), which restricts the detection of Fe^{3+} ions through CPL channel.

The S4-BC resulting from bacterial fermentation of S4, inherits the near-infrared emissive character of S4 and displays near-infrared CPL (Fig. 6d). Therefore, we proposed that S4-BC can serve as a chiral sensing platform for Fe^{3+} ions detection through ratiometric fluorescent and CPL channels (Fig. 9a). However, the response rate of
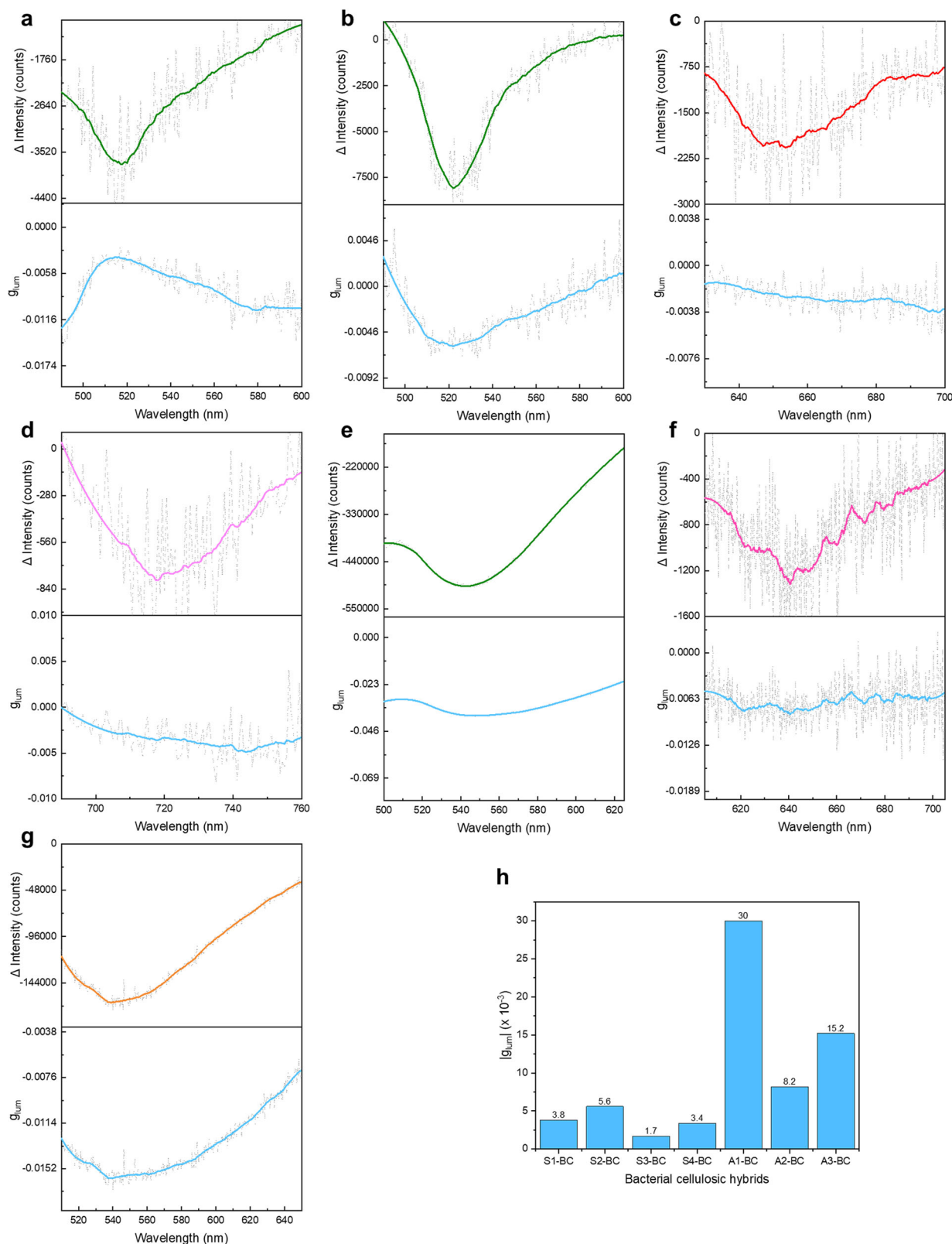
Fig. 6 | CPL performance of bacterial cellulosic biofilms. CPL spectra from CPL-silent glycosylated dyes. For S1-BC (**a**) and S2-BC (**b**), λ_{ex} = 370 nm, for S3-BC (**c**), λ_{ex} = 580 nm, and for S4-BC (**d**), λ_{ex} = 650 nm. CPL spectra from CPL-active glycosylated luminophores. For A1-BC (**e**) and A3-BC (**g**), λ_{ex} = 370 nm, and for A2-BC (**f**), λ_{ex} = 550 nm. **h** Summary of g_{lum} of all bacterial cellulosic biofilms. (**a**–**g** the gray dot curves are the original collected data, while the solid curves are the smoothed ones.) CPL, circularly polarized luminescence. Source data are provided as a Source Data file.
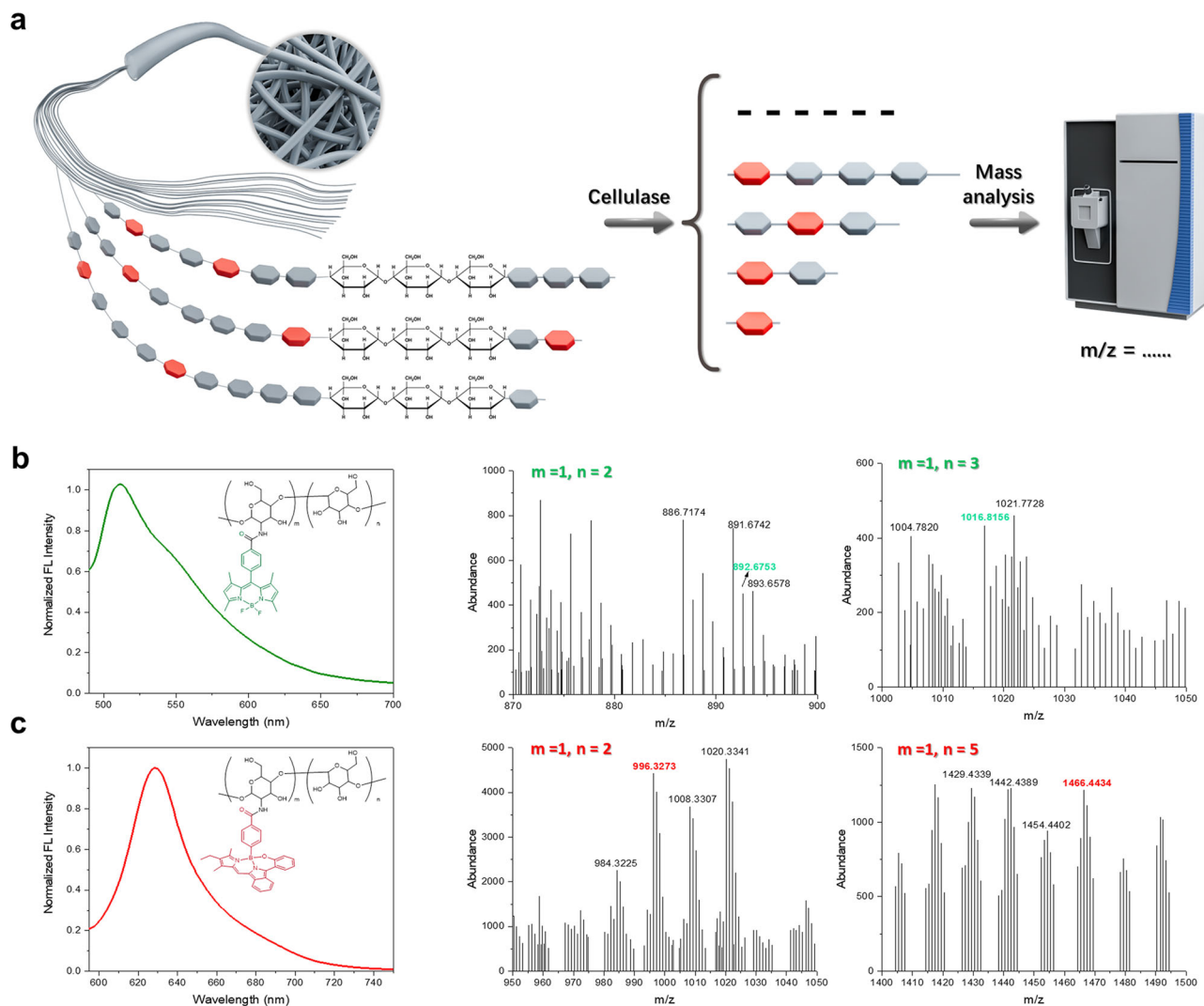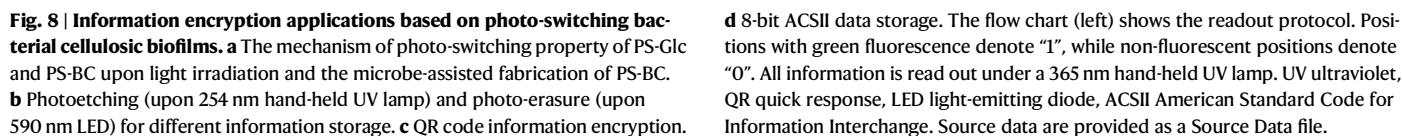
Fig. 7 | Confirmation of covalent bond formation during bacterial copolymerization of glucose and glycosylate dyes. a Schematic representation of the confirmation process with the help of cellulase-catalyzed biodegradation (S3-BC as an example). **b** Fluorescence spectrum (left) and representative mass analysis (right) of hydrolysate for S2-BC. HRMS in the positive ion reflective mode demonstrated the $[M + K]^+$ peak of S2-hybrid cellobiose ($m = 1$, $n = 2$) and $[M + H]^+$ peak of S2-hybrid cellotriose ($m = 1$, $n = 3$) at a mass-to-charge ratio (m/z) of 892.6753 and 1016.8156, respectively. **c** Fluorescence spectrum (left) and representative mass analysis (right) of hydrolysate for S3-BC. HRMS in the positive ion reflective mode demonstrated the $[M + K]^+$ peak of S3-hybrid cellobiose ($m = 1$, $n = 2$) and $[M + Na]^+$ peak of S3-hybrid cellopentaose ($m = 1$, $n = 5$) at a mass-to-charge ratio (m/z) of 996.3273 and 1466.4434, respectively. HRMS, high-resolution mass spectrometry. Source data are provided as a Source Data file.

S4-BC to Fe^{3+} ions is unsatisfactory due to adsorption and limited molecular collisions, restricting its potential application (Fig. 9b). Interestingly, we discovered that this response process was accelerated with the assistance of 420 nm blue light (Fig. 9c), while the fluorescence changes of S4-BC without Fe^{3+} ions were negligible in comparison (Fig. 9d). Through electron paramagnetic resonance (EPR) experiments, we discovered that the superoxide anion radical ($\cdot O_2^-$), singlet oxygen ($^1O_2$), and hydroxyl radical ($\cdot OH^-$) were generated during this process (Fig. 9e–g). However, no radicals were generated when S4-BC was exposed to 420 nm light (Supplementary Fig. 26a–c). Additionally, we found that radicals were only generated in the combination of bacterial cellulose and Fe^{3+} ions (Supplementary Fig. 26d–l), demonstrating the important role of hydroxyl-rich bacterial cellulose. We hypothesize the hydroxyl group in bacterial cellulose might help form the Fe^{3+}- BC intermediate, releasing radicals under blue light irradiation and enhancing alkene oxidative cleavage[72]. Therefore, these results indicate that blue light can accelerate the Fe^{3+} catalyzed reactive oxygen species (ROS) generation in the bacterial cellulose, thereby improving Fe^{3+} ions sensing on

S4-BC. As anticipated, the detection of Fe^{3+} ions via the CPL channel was successfully achieved. After reacting with Fe^{3+} ions with the assistance of 420 nm light, the Left and Right CPL, and the intensity difference between Left and Right CPL (Δ intensity), shifted from the near-infrared CPL window (Figs. 9h–j) to the red CPL window (Fig. 9k–m), enabling ratiometric detection of Fe^{3+} ions through the CPL channel. Therefore, by integrating S4 and S4-BC, we have achieved dual-channel ratiometric sensing of Fe^{3+} ions based on fluorescence and CPL.

In summary, we have achieved in situ bacterial copolymerization of broad-spectrum glycosylated luminophores, which is an efficient biosynthetic strategy for CPL-active material fabrication. This strategy is based on cellulose synthases catalyzing the β-1,4-glycosidic reaction of glucose monomers and glycosylated luminophores in situ. Subsequently, we have used it to embed green, red, orange, and near infrared glycosylated luminophores into bacterial cellulose with good universality. Interestingly, this approach can significantly induce CPL emission for CPL-silent glycosylated luminophores with a g_{lum} up to -5.6×10^{-3} and can also significantly enhance CPL

Fig. 8 | Information encryption applications based on photo-switching bacterial cellulosic biofilms. a The mechanism of photo-switching property of PS-Glc and PS-BC upon light irradiation and the microbe-assisted fabrication of PS-BC. **b** Photoetching (upon 254 nm hand-held UV lamp) and photo-erasure (upon 590 nm LED) for different information storage. **c** QR code information encryption. **d** 8-bit ACSII data storage. The flow chart (left) shows the readout protocol. Positions with green fluorescence denote "1", while non-fluorescent positions denote "0". All information is read out under a 365 nm hand-held UV lamp. UV ultraviolet, QR quick response, LED light-emitting diode, ACSII American Standard Code for Information Interchange. Source data are provided as a Source Data file.

performance for CPL-active glycosylated luminophores, amplifying the g_{lum} from the 10^{-4} scale to 10^{-2} and 10^{-3} by as much as 39-fold. Moreover, a direct method is explored for the characterization of bacterial cellulosic hybrids, confirming the covalent bond formation during bacterial copolymerization between glucose and glycosylated luminophores. By taking the advantage of photo-switching molecule, the information encryption models based on fluorescent bacterial cellulosic biofilms is proposed. More importantly, the detection of Fe^{3+} ion through fluorescence and CPL channels using S4 and S4-BC is successfully realized. Collectively, this study not only achieves bacterial copolymerization of a broad spectrum of functional molecules for multicolor CPL and fabricates photo-switching and sensing materials but also broadens the applications of bacterial cellulosic hybrids.

Methods

General

All reagents and solvents were obtained from commercial suppliers and were used without further purification. The ^{1}H NMR and ^{13}C NMR spectra were recorded using a Bruker AV-400 instrument (Bruker, Germany), with results reported in ppm downfield. High-resolution mass spectra (HRMS) were obtained using a Xevo G2-XSQT spectrometer (Waters, UK), Bruker Microflex MALDI-TOF system, and Agilent Q-TOF 6550 system. UV−Vis absorption and fluorescence spectroscopy measurements were conducted using a UV spectrophotometer (UV-1800, Shimadzu, Japan) and a fluorescence spectrophotometer (Horiba Fluorolog-3, Horiba, Japan). The absolute fluorescence quantum yields and lifetimes were conducted using Fluorolog-3 fluorescence spectrophotometer (Horiba, Japan).
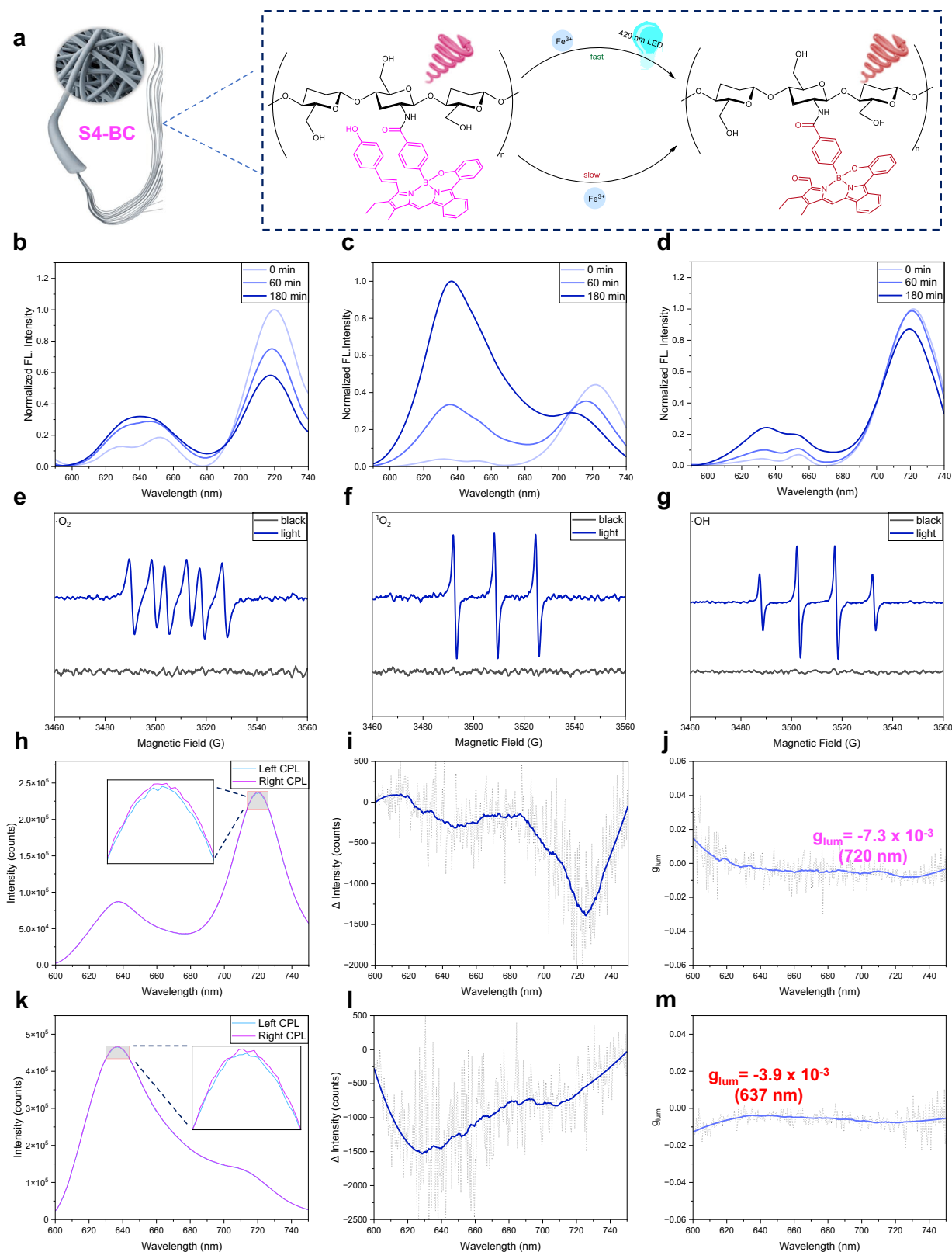
Fig. 9 | Fluorescent and circularly polarized luminescent dual-sensing Fe^{3+} ions base on S4-BC. a Schematic representation of the process for fluorescent and CPL dual-sensing Fe^{3+} ions in S4-BC. **b** Normalized fluorescence changes of S4-BC upon addition of Fe^{3+} ions (162 μg/mL, 700 μL). **c** Normalized fluorescence changes of S4-BC upon addition of Fe^{3+} ions (162 μg/mL, 700 μL) with assistance of a 420 nm LED (4 mM/cm²). **d** Normalized fluorescence changes of S4-BC (in Milli-Q water, 700 μL) upon exposure to a 420 nm LED (4 mM/cm²). **e–g** Electron paramagnetic resonance (EPR) results for S4-BC in Fe^{3+} solution under 420 nm light irradiation or not.

Superoxide anion radical ($\cdot O_2^-$, **e**), singlet oxygen ($^1O_2$, **f**), and hydroxyl radical ($\cdot OH^-$, **g**). **h–j** CPL performance of S4-BC in Milli-Q water (700 μL). **k–m** CPL performance of S4-BC after reacting with Fe^{3+} ions with assistance of a 420 nm LED (4 mM/cm²). λ_{ex} = 400 nm. (**i**, **j**, and **l**, **m**: the gray dot curves are the original collected data, while the solid curves are the smoothed ones.) LED light-emitting diode, $\cdot O_2^-$ superoxide radical, $^1O_2$ singlet oxygen, $\cdot OH^-$ hydroxyl radical. Source data are provided as a Source Data file.

The fluorescence lifetimes were analyzed using the Horiba DAS6 software. Confocal imaging experiments were performed using a confocal laser scanning microscope (CLSM, Carl Zeiss LSM710, Germany). The morphology of the bacterial cellulose and bacterial cellulosic hybrids were characterized using a field emission scanning electron microscope (Zeiss Sigma FESEM, Germany). Transmembrane I−V curves were recorded using a Keithley 6487 pm and a control computer. Gel permeation choromatogarphy (GPC) experiments were conducted using the Agilent GPC50 system equipped with a PLgel 10 µm MIXED-B column. The electron paramagnetic resonance (EPR) measurements were conducted using a Bruker Model A300. OD_{600} (optical density) values were recorded using Cytation 3 Imaging Reader. Circular dichroism experiments were conducted using Applied Photophysics Chirascan™ Circular Dichroism (CD) Spectrometer. Circularly polarized luminescence (CPL) spectra were recorded using the Olis CPL Solo system.

Strains and culture medium

Acetobacter xylinus (*Komagataeibacter sucrofermentants* ATCC700178) were used for bacterial fermentation. The culture medium consisted of glucose 50 g/L, yeast extract 5 g/L, calcium carbonate 12.5 g/L, and were sterilized at 121 °C for 30 min.

Preparation of bacterial cellulosic biofilms

Komagataeibacter sucrofermentans were cultivated in a culture medium enriched with various glycosylated dyes. The concentration of these glycosylated dyes was 10 mg (20 mg for PS-Glc, dissolved in 1 mL DMSO) per 100 mL of the medium. The fermentation process was carried out in 250 mL autoclaved baker at a temperature of 26 °C and lasted for 6 days (12 days for A3). Following this, the resulting bacterial cellulose and hybrid bacterial cellulosic biofilms were treated with a 1 wt% sodium hydroxide (NaOH) solution at 60 °C for a duration of 5 h to eliminate bacteria and proteins. Subsequently, the treated materials were thoroughly rinsed with deionized water until the pH stabilized at 7.0 and no fluorescence could be detected in the wash water. Finally, all the bacterial cellulose samples were dried in an oven at 65 °C for scanning electron microscopy (SEM) characterization and circularly polarized luminescence (CPL) performance evaluation.

Current-voltage experiment

The experiments were performed in a 0.1 nM KCl aqueous solution with a pH of 7.0. The picoammeter was used as a voltage source to facilitate transmembrane ionic transport. The scanning voltage ranged from −1 V to +1 V, with increments of 100 mV.

Circular polarized luminescence performance evaluation system setup

Circular polarized luminescence (CPL) spectra were measured with the Olis CPL Solo system.

For S1 and S2, bandpass: 0.5, excitation at 370 nm, spectra are taken as an average of 10 scans with a 5 s integration time. For S3, bandpass: 0.5, excitation at 500 nm, spectra are taken as an average of 10 scans with a 5 s integration time. For S4, bandpass: 5, excitation at 650 nm, spectra are taken as an average of 30 scans with a 5 s integration time. For A1, bandpass: 5, excitation at 450 nm, spectra are taken as an average of 30 scans with a 1 s integration time. For A2, bandpass: 5, excitation at 580 nm, spectra are taken as an average of 30 scans with a 1 s integration time. For A3, bandpass: 2.4, excitation at 370 nm, spectra are taken as an average of 20 scans with a 2 s integration time.

For S1-BC and S2-BC, bandpass: 1.5, excitation at 370 nm, spectra are taken as an average of 10 scans with a 5 s integration time. For S3-BC, bandpass: 5, excitation at 580 nm, spectra are taken as an average of 15 scans with a 5 s integration time. For S4-BC, bandpass: 5, excitation at 650 nm, spectra are taken as an average of 30 scans with a 5 s integration time. For A1-BC, bandpass: 1.5, excitation at 370 nm. Spectra are taken as an average of 20 scans with a 5 s integration time. For A2-BC, bandpass: 5, excitation at 550 nm. spectra are taken as an average of 25 scans with a 2 s integration time. For A3-BC, bandpass: 2.4, excitation at 370 nm. spectra are taken as an average of 16 scans with a 2 s integration time.

Cellulase-catalyzed biodegradation of bacterial cellulosic biofilms

Bacterial cellulose biofilm was cut into small pieces and were suspended in deionized water with a pH of 5.5 in a 50 mL flask. Cellulase was then added to this mixture, and it was stirred and hydrolyzed at a temperature of 50 °C for 48 h (S2-BC, 24 h for S3-BC). Following hydrolysis, methanol was added to the hydrolysate, and the resulting solution was quickly purified using a silica plug to remove insoluble substances. The methanol-water mixture was collected for analysis using high resolution mass spectrometry and fluorescence emission spectroscopy.

High-resolution mass spectrometry

To monitor the cellulase-catalyzed biodegradation of bacterial cellulosic biofilms (S2-BC and S3-BC), HRMS experiments were conducted using an Agilent Q-TOF 6550 system. The mobile phases consisted of 80% methanol and 20% water. Samples from the cellulase-catalyzed biodegradation process, dissolved in a methanol/water mixture, were filtered through a 0.22 µm Nylon 66 filtration membrane. The injection volume was 1 µL, with a flow rate of 0.3 mL/min. ESI source parameters included a gas temperature of 150 °C and a drying gas flow rate of 15 L/min, a sheath gas temperature of 350 °C with a sheath gas flow of 12 L/min. The ESI positive mode operated within a mass range of 50–3000 m/z at a voltage of 4000 V. Data files were exported using MassHunter software, the resulting data were analyzed using Microsoft Excel 2016 and Origin 2024 software with default settings.

To characterize the relevant synthesized compounds (Supplementary Figs. 1–8) in this study, HRMS experiments were conducted using Waters Xevo G2-XSQT spectrometer or Bruker Microflex MALDI-TOF system. All the samples dissolved in methanol and filtered through a 0.22 µm Nylon 66 filtration membrane. MALDI-TOF experiments were performed using CHCA (α-cyano-4-hydroxycinnamic acid) as the matrix, with 2000 satisfactory shots in 250 shot steps. The acquisition settings were as follows: initial laser power set at 30%, maximum laser power at 100%, detector gain voltage for linear base set to 2500 V, and detector gain voltage for reflector base set to 1400 V. Data were analyzed and exported using flexAnalysis software with default settings. LC-MS was performed on a Waters Xevo G2-XSQT spectrometer with an ACQUITY UPLC BEH C18 column (2.1 × 50 mm, 1.7 µm), using mobile phases of methanol and water supplemented with 0.1% formic acid. The gradient was 30% methanol for 1 min, 30% to 100% methanol over 1 min, 100% methanol for 3 min, 100% to 30% methanol over 0.5 min, and 30% methanol for 1.5 min. The flow rate was maintained at 0.4 mL/min throughout the run. The ESI source parameters were set to a cone temperature of 120 °C, a gas flow rate of 50 L/h, and a capillary voltage of 3000 V. Data acquisition and processing were performed using MassLynx software with default settings.

Fe^{3+} ions detection based on S4-BC

The fluorescence and CPL performance of S4-BC before and after reacting with Fe^{3+} ions were evaluated in Milli-Q water (700 µL) and Fe^{3+} solution (162 µg/mL, 700 µL), respectively, with 400 nm light excitation.

CPL performance evaluation system setup for S4-BC: bandpass: 5, excitation at 400 nm, spectra are taken as an average of 20 scans with a 1 s integration time.

CPL performance evaluation system setup for S4-BC after reacting with Fe^{3+} ions: bandpass: 5, excitation at 400 nm, spectra are taken as an average of 30 scans with a 1 s integration time.

Gel permeation chromatography (GPC) experiment

The bacterial cellulose biofilms and hybrid bacterial cellulose biofilms were cut into small pieces. Subsequently, 15 mg of these pieces were dispersed in a 1.5 mL LiCl/DMAc solution (5:1, w/v). The resulting mixture was gradually heated from room temperature to 150 °C over a period of 1.5 h under continuous stirring. Following this, the mixture was maintained at 150 °C for an additional 20 min. After that, the mixture was cooled to 65 °C with stirring until a viscous liquid formed. The molecular weights of the resulting viscous liquids were assessed using the Agilent GPC50 system equipped with a PLgel 10 μm MIXED-B column. The analysis was performed at a flow rate of 1 mL/min and a temperature of 50 °C, using DMAC with 0.5% LiCl as the eluent. The molecular weights were summarized in Supplementary Table 3.

Electron paramagnetic resonance (EPR) experiment

The EPR measurements were conducted using a Bruker Model A300 at ambient temperature. All samples were prepared under identical conditions, using BC (S4-BC or $FeCl_3$ solution) and either DMPO (5,5-dimethyl-1-pyrroline N-oxide) or TEMP (2,2,6,6-Tetramethylpiperidine). A 420 nm light source was employed for different samples. Prior to the EPR spectra measurements, the samples were exposed to light for 10 min. Control groups were prepared in the same manner but without any light exposure.

Statistics and reproducibility

Bacterial fermentation experiments for all glycosylated molecules were repeated three times, and all attempts at replication were successful to fabricate bacterial cellulosic hybrids. The characterization experiments of Fig. 4c, d were repeated three times independently with similar results. No statistical method was used to predetermine sample size. No data were excluded from the analyses.

Reporting summary

Further information on research design is available in the Nature Portfolio Reporting Summary linked to this article.

Data availability

The data that supports the findings of this study can be found in the manuscript and its Supplementary Information. Source data are provided with this paper.

References

1. Wagenknecht, C. et al. Experimental demonstration of a heralded entanglement source. Nature Photon. 4, 549–552 (2010).
2. Mao, N. et al. Nonlinear diatomic metasurface for real and fourier space image encoding. Nano. Lett. 20, 7463–7468 (2020).
3. Josse, P. et al. Enantiopure versus racemic naphthalimide end-capped helicenic non-fullerene electron acceptors: impact on organic photovoltaics performance. Chem. Eur. J. 23, 6277–6281 (2017).
4. Li, M. et al. Stable enantiomers displaying thermally activated delayed fluorescence: efficient oleds with circularly polarized electroluminescence. Angew. Chem. Int. Ed. 57, 2889–2893 (2018).
5. Han, J. et al. Recent progress on circularly polarized luminescent materials for organic optoelectronic devices. Adv. Optical Mater. 6, 1800538 (2018).
6. Yang, Y., da Costa, R. C., Fuchter, M. J. & Campbell, A. J. Circularly polarized light detection by a chiral organic semiconductor transistor. Nature Photon. 7, 634–638 (2013).
7. Wang, S. et al. Self-reporting activated ester-amine reaction for enantioselective multi-channel visual detection of chiral amines. Angew. Chem. Int. Ed. 61, e202202268 (2022).
8. Fan, H. et al. ATP-induced emergent circularly polarized luminescence and encryption. Angew. Chem. Int. Ed. 61, e202200727 (2022).
9. Shuvaev, S., Fox, M. A. & Parker, D. Monitoring of the ADP/ATP ratio by induced circularly polarised europium luminescence. Angew. Chem. Int. Ed. 57, 7488–7492 (2018).
10. Maeda, H. et al. Chemical-stimuli-controllable circularly polarized luminescence from anion-responsive pi-conjugated molecules. J. Am. Chem. Soc. 133, 9266–9269 (2011).
11. Gong, J. et al. Iodization-enhanced fluorescence and circularly polarized luminescence for dual-readout probe design. Sensor. Actuat. B Chem. 347, 130610 (2021).
12. Zhang, L., Wang, H. X., Li, S. & Liu, M. Supramolecular chiroptical switches. Chem. Soc. Rev. 49, 9095–9120 (2020).
13. Lin, S., Gutierrez-Cuevas, K. G., Zhang, X., Guo, J. & Li, Q. Fluorescent photochromic α-cyanodiarylethene molecular switches: an emerging and promising class of functional diarylethene. Adv. Funct. Mater. 31, 2007957 (2020).
14. Kim, Y. et al. Reconfigurable chiroptical nanocomposites with chirality transfer from the macro- to the nanoscale. Nat. Mater. 15, 461–468 (2016).
15. Chen, Y. et al. ESIPT-inspired dual-mode photoswitches with fast molecular isomerization in the solid state. Angew. Chem. Int. Ed. 135, e202301765 (2023).
16. Yang, G. et al. A flexible circularly polarized luminescence switching device based on proton-coupled electron Transfer. Adv. Sci. 9, e2202636 (2022).
17. Stachelek, P., MacKenzie, L., Parker, D. & Pal, R. Circularly polarised luminescence laser scanning confocal microscopy to study live cell chiral molecular interactions. Nat. Commun. 13, 553 (2022).
18. Zhao, T., Duan, P., & Liu, M. Circularly polarized luminescence from gelator molecules: from isolated molecules to assemblies. (Springer, Singapore, 2020).
19. Sanchez-Carnerero, E. M. et al. Circularly polarized luminescence from simple organic molecules. Chem. Eur. J. 21, 13488–13500 (2015).
20. Zhao, W. L., Li, M., Lu, H. Y. & Chen, C. F. Advances in helicene derivatives with circularly polarized luminescence. Chem. Commun. 55, 13793–13803 (2019).
21. Arrico, L., Di Bari, L. & Zinna, F. Quantifying the overall efficiency of circularly polarized emitters. Chem. Eur. J. 27, 2920–2934 (2021).
22. Tang, X. et al. Endohedral functionalization of chiral metal-organic cages for encapsulating achiral dyes to induce circularly polarized luminescence. Chem. 7, 2771–2786 (2021).
23. Wu, K., Tessarolo, J., Baksi, A. & Clever, G. H. Guest-modulated circularly polarized luminescence by ligand-to-ligand chirality transfer in heteroleptic Pd(II) coordination cages. Angew. Chem. Int. Ed. 61, e202205725 (2022).
24. Gong, J. & Zhang, X. Coordination-based circularly polarized luminescence emitters: design strategy and application in sensing. Coord. Chem. Rev. 453, 214329 (2022).
25. Full, J., Panchal, S. P., Gotz, J., Krause, A. M. & Nowak-Krol, A. Modular synthesis of organoboron helically chiral compounds: cutouts from extended helices. Angew. Chem. Int. Ed. 60, 4350–4357 (2021).
26. Sanchez-Carnerero, E. M. et al. Circularly polarized luminescence by visible-light absorption in a chiral O-BODIPY dye: unprecedented design of CPL organic molecules from achiral chromophores. J. Am. Chem. Soc. 136, 3346–3349 (2014).
27. Greenfield, J. L. et al. Pathways to increase the dissymmetry in the interaction of chiral light and chiral molecules. Chem. Sci. 12, 8589–8602 (2021).

28. Sang, Y., Han, J., Zhao, T., Duan, P. & Liu, M. Circularly polarized luminescence in nanoassemblies: generation, amplification, and application. *Adv. Mater.* **32**, e1900110 (2020).

29. Zhao, T., Han, J., Duan, P. & Liu, M. New perspectives to trigger and modulate circularly polarized luminescence of complex and aggregated systems: energy transfer, photon upconversion, charge transfer, and organic radical. *Acc. Chem. Res.* **53**, 1279–1292 (2020).

30. Liu, M., Zhang, L. & Wang, T. Supramolecular chirality in self-assembled systems. *Chem. Rev.* **115**, 7304–7397 (2015).

31. Du, C., Li, Z., Zhu, X., Ouyang, G. & Liu, M. Hierarchically self-assembled homochiral helical microtoroids. *Nat. Nanotechnol.* **17**, 1294–1302 (2022).

32. Kotova, O. et al. Lanthanide luminescence from supramolecular hydrogels consisting of bio-conjugated picolinic-acid-based gua-nosine quadruplexes. *Chem.* **8**, 1395–1414 (2022).

33. Zhang, C., Li, Z. S., Dong, X. Y., Niu, Y. Y. & Zang, S. Q. Multiple responsive CPL switches in an enantiomeric pair of perovskite confined in lanthanide MOFs. *Adv. Mater.* **34**, e2109496 (2022).

34. Shang, W. et al. Chiral reticular self-assembly of achiral AIEgen into optically pure metal-organic frameworks (MOFs) with dual mechano-switchable circularly polarized luminescence. *Angew. Chem. Int. Ed.* **59**, 12811–12816 (2020).

35. Yang, X., Jin, X., Zhao, T. & Duan, P. Circularly polarized luminescence in chiral nematic liquid crystals: generation and amplification. *Mater. Chem. Front.* **5**, 4821–4832 (2021).

36. Wang, X., Zhao, B. & Deng, J. Liquid crystals doped with chiral fluorescent polymer: multi-color circularly polarized fluorescence and room-temperature phosphorescence with high dissymmetry factor and anti-counterfeiting application. *Adv. Mater.* **35**, 2304405 (2023).

37. Wu, Y., Li, M., Zheng, Z. G., Yu, Z. Q. & Zhu, W. H. Liquid crystal assembly for ultra-dissymmetric circularly polarized luminescence and beyond. *J. Am. Chem. Soc.* **145**, 12951–12966 (2023).

38. Kang, W. et al. Photo- and thermo-driven azoarene-based circularly polarized luminescence molecular switch in liquid crystal host. *Angew. Chem. Int. Ed.* **135**, e202311486 (2023).

39. Zheng, H. et al. Uncovering the circular polarization potential of chiral photonic cellulose films for photonic applications. *Adv. Mater* **30**, e1705948 (2018).

40. Zou, C. et al. Bacterial cellulose: a versatile chiral host for circularly polarized luminescence. *Molecules* **24**, 1008 (2019).

41. Xu, M. et al. Exploring the circular polarization capacity from chiral cellulose nanocrystal films for a photo-controlled chiral helix of supramolecular polymers. *Angew. Chem. Int. Ed.* **61**, e202117042 (2022).

42. Takaishi, K., Iwachido, K., Takehana, R., Uchiyama, M. & Ema, T. Evolving fluorophores into circularly polarized luminophores with a chiral naphthalene tetramer: proposal of excimer chirality rule for circularly polarized luminescence. *J. Am. Chem. Soc.* **141**, 6185–6190 (2019).

43. Han, J., Shi, Y., Jin, X., Yang, X. & Duan, P. Regulating the excited state chirality to fabricate high-performance-solid-state circularly polarized luminescence materials. *Chem. Sci.* **13**, 6074–6080 (2022).

44. Kumar, J., Nakashima, T. & Kawai, T. Circularly polarized luminescence in chiral molecules and supramolecular assemblies. *J. Phys. Chem. Lett.* **6**, 3445–3452 (2015).

45. Deng, Y. et al. Circularly polarized luminescence from organic micro-/nano-structures. *Light. Sci. Appl.* **10**, 76 (2021).

46. Roose, J., Tang, B. Z. & Wong, K. S. Circularly-polarized luminescence (CPL) from chiral AIE molecules and macrostructures. *Small* **12**, 6495–6512 (2016).

47. Winter, J. M. & Tang, Y. Synthetic biological approaches to natural product biosynthesis. *Curr. Opin. Biotechnol.* **23**, 736–743 (2012).

48. Bornscheuer, U. T. et al. Engineering the third wave of biocatalysis. *Nature* **485**, 185–194 (2012).

49. Zhang, Y. H. Production of biofuels and biochemicals by in vitro synthetic biosystems: opportunities and challenges. *Biotechnol. Adv.* **33**, 1467–1483 (2015).

50. Sheldon, R. A. & Brady, D. The limits to biocatalysis: pushing the envelope. *Chem. Commun.* **54**, 6088–6104 (2018).

51. Zhang, X. et al. Synthesizing biomaterials in living organisms. *Chem. Soc. Rev.* **52**, 8126–8164 (2023).

52. Lin, S. et al. Surface-modified bacteria: synthesis, functionalization and biomedical applications. *Chem. Soc. Rev.* **52**, 6617–6643 (2023).

53. Bennett, M. R., Gurnani, P., Hill, P. J., Alexander, C. & Rawson, F. J. Iron-catalysed radical polymerisation by living bacteria. *Angew. Chem. Int. Ed.* **59**, 4750–4755 (2020).

54. Mishra, S. et al. Biochemistry, synthesis, and applications of bacterial cellulose: a review. *Front. Bioeng. Biotechnol.* **10**, 780409 (2022).

55. Gao, M. et al. A natural in situ fabrication method of functional bacterial cellulose using a microorganism. *Nat. Commun.* **10**, 437 (2019).

56. Liu, C. et al. Biological synthesis and process monitoring of an aggregation-induced emission luminogen-based fluorescent polymer. *JACS Au* **2**, 2162–2168 (2022).

57. Liu, X. et al. Direct synthesis of photosensitizable bacterial cellulose as engineered living material for skin wound repair. *Adv. Mater.* **34**, e2109010 (2022).

58. Babi, M. et al. Unraveling the supramolecular structure and nanoscale dislocations of bacterial cellulose ribbons using corre-lative super-resolution light and electron microscopy. *Biomacro-molecules* **24**, 258–268 (2022).

59. Jimenez, J. et al. Modulating ICT emission: a new strategy to manipulate the CPL sign in chiral emitters. *Chem. Commun.* **55**, 1631–1634 (2019).

60. Gong, Z.-L. et al. Frontiers in circularly polarized luminescence: molecular design, self-assembly, nanomaterials, and applications. *Sci. China Chem.* **64**, 2060–2104 (2021).

61. Manan, S. et al. Bacterial cellulose: molecular regulation of bio-synthesis, supramolecular assembly, and tailored structural and functional properties. *Prog. Mater. Sci.* **129**, 100972 (2022).

62. Saritha Mohanram, V. R. Beta-glucosidase: key enzyme in deter-mining efficiency of cellulase and biomass hydrolysis. *J. Biopro-cess. Biotech.* **5**, 1000197 (2015).

63. Irie, M. Diarylethenes for memories and switches. *Chem. Rev.* **100**, 1685–1716 (2000).

64. Irie, M., Fukaminato, T., Matsuda, K. & Kobatake, S. Photochromism of diarylethene molecules and crystals: memories, switches, and actuators. *Chem. Rev.* **114**, 12174–12277 (2014).

65. Li, M. et al. Light-driven chiral switching of supramolecular metal-lacycles with photoreversibility. *Chem.* **5**, 634–648 (2019).

66. Poon, C. T., Lam, W. H., Wong, H. L. & Yam, V. W. A versatile pho-tochromic dithienylethene-containing beta-diketonate ligand: near-infrared photochromic behavior and photoswitchable lumi-nescence properties upon incorporation of a boron(III) center. *J. Am. Chem. Soc.* **132**, 13992–13993 (2010).

67. Zheng, Z. et al. Digital photoprogramming of liquid-crystal super-structures featuring intrinsic chiral photoswitches. *Nature Photon.* **16**, 226–234 (2022).

68. Pan, Y., Zhang, C., Liu, S. H., Tan, Y. & Yin, J. Fluorescent switch based on dithienylethene with dansulfonamide in multimedium. *Dyes Pigments* **181**, 108546 (2020).

69. Imai, Y., Nakano, Y., Kawai, T. & Yuasa, J. A smart sensing method for object identification using circularly polarized luminescence from coordination-driven self-assembly. *Angew. Chem. Int. Ed.* **57**, 8973–8978 (2018).

70. Lu, D. et al. Cellulose nanocrystal films with NIR-II circularly polarized light for cancer detection applications. *ACS Nano*. **17**, 461–471 (2023).
71. Wang, C. et al. Self-Immolative photosensitizers for self-reported cancer phototheranostics. *J. Am. Chem. Soc.* **145**, 13099–13113 (2023).
72. Majumder, P. et al. Enhanced alkene oxidative cleavage in water via photoexcited FeIV species within covalent organic framework thin films. *Angew. Chem. Int. Ed.* **63**, e202412122 (2024).

Acknowledgements

Author contributions

Y.S. and X.Z. conceived the idea and designed the experiments. Y.S., J.L., C.W. (Wang), and J.G. synthesized the glycosylated molecules and conducted characterizations. Y.S. and D.Z. conducted the transmembrane current experiments and SEM characterizations. Y.S. and Z.D. performed the bacterial copolymerization experiments. Y.S. conducted other experiments. X.Z. supervised the project. X.Z., K.H.W., and C.W. (Wu) acquired project funding. Y.S. and X.Z. wrote the paper. All authors analyzed the data, discussed the results, commented on and revised the manuscript.

Competing interests

The authors declare no competing interests.

Additional information